S1 Model description

To determine the canopy temperature, we developed a model considering the whole canopy as subject to the same conditions, with single exchange fluxes of energy and mass ('big-leaf model'; Tuzet et al., 2003; Bonan, 2019; Amthor, 1994; Jarvis and McNaughton, 1986), and uniform soil features and water content over the active rooting zone ('bucket filling model';
5 Rodriguez-Iturbe et al., 1999; Laio et al., 2001; Milly, 1994). For set conditions above the canopy (radiation, wind velocity, air temperature and vapor pressure deficit), the model quantifies the canopy energy and water balances (Section S1.1-1.2), as a function of the canopy water potential. In turn, the canopy water potential was determined by the soil water balance and transport of water from the soil, inside the canopy to the atmosphere (Section S1.3). The whole system was forced by the conditions above the canopy and the precipitation input to the soil water balance, which were synthetically generated (Section
10 S1.4). All the mathematical symbols are defined in Table S1. The model parameters are summarized in Table S2.

S1.1 Canopy conditions

S1.1.1 Radiation

To determine the canopy energy balance, a simplified radiation model was used, accounting for visible, near-infrared, and longwave radiation separately (Goudriaan and Van Laar, 1994; Leuning et al., 1995). All fluxes were expressed on a per unit
15 ground area basis.

Shortwave radiation

The incoming shortwave radiation at the top of the canopy, $Q_0^\downarrow$, was partitioned into the near infrared (NIR) and visible (PAR) components, $Q_{0,NIR}^\downarrow$ and $Q_{0,PAR}^\downarrow$, based on the fractions f_{NIR} and f_{PAR} respectively.

20 By integrating the radiation absorbed by each canopy layer within a canopy, assuming constant leaf area density (Goudriaan and Van Laar, 1994; Bonan, 2019), the total radiation absorbed by the canopy for component *i* (with *i*=NIR, PAR) was determined as (Tuzet et al., 2003):

$$Q_i^\downarrow = Q_{0,i}^\downarrow (1 - \rho_i) \left[1 - exp\left(-K_{bl} \sqrt{1 - \sigma_i} \, L_{AI}\right) \right],\tag{S1}$$

where $Q_{0,i}^\downarrow$ is the solar radiation above the canopy in the corresponding component, ρ_i is the canopy reflection coefficient, K_{bl} is the extinction coefficient for black leaves, σ_i is the leaf scattering coefficient (so that $K_{bl} \sqrt{1 - \sigma_i}$ represents the effective
25 transmission coefficient), and L_{AI} is the canopy leaf area index.

The canopy extinction coefficient for black leaves depends on the direction of radiation and leaf orientation. Assuming an isotropic leaf angle distribution, it can be obtained as (Goudriaan and Van Laar, 1994)

$$K_{bl} = \frac{1}{2 \cos \theta_{sun}},\tag{S2}$$

where θ_{sun} is the solar zenith angle, determined based on the field location, day of the year, and time of the day (Dingman, 1994).

30 The canopy reflection coefficient for PAR (*i*=PAR) and NIR (*i*=NIR) was calculated as (Goudriaan and Van Laar, 1994)

$$\rho_i = 2K_{bl}\big(K_{bl} + K_{bl,d}\big)^{-1}\big(1 - \sqrt{1 - \sigma_i}\big)\big(1 + \sqrt{1 - \sigma_i}\big)^{-1}. \tag{S3}$$

where $K_{bl,d}$ is the extinction coefficient for diffuse radiation.

The total net shortwave radiation absorbed by the canopy is thus sum of the PAR and NIR components, $Q^{\downarrow} = Q_{PAR}^{\downarrow} + Q_{NIR}^{\downarrow}$.

Thermal (longwave) radiation

The net absorbed longwave radiation is the difference between the sky downward thermal radiation and the canopy upward emissivity (Leuning et al., 1995; Goudriaan and Van Laar, 1994):

$$B_n^{\downarrow} = \big(\varepsilon_a \sigma T_a^4 - \varepsilon_c \sigma T_c^4\big)\big[1 - exp\big(-K_{bl,d}\ L_{AI}\big)\big] \cong B_{n,ref}^{\downarrow} + \Delta B^{\downarrow}, \tag{S4}$$

where ε_a is the apparent emissivity for a hemisphere radiating at temperature T_a (Campbell and Norman, 1998), ε_c is the canopy emissivity, σ is the Stefan-Boltzmann constant, T_a and T_c are the air and canopy temperatures respectively (expressed in Kelvin). As in Eq. (S1), the term in square brackets is the result of integrating the fluxes over the whole canopy height (Bonan, 2019), although considering the black leaf transmissivity for thermal radiation $K_{bl,d}$. The simplifying assumption was made that the longwave radiation exchange between the bottom of the canopy and the soil surface is negligible, because, under closed canopy, the soil temperature is similar to that of the canopy. The apparent emissivity depends on the cloud cover as $\varepsilon_a = \varepsilon_{a,clear}(1 - 0.84\ f_{cloud}) + 0.84\ f_{cloud}$, where $\varepsilon_{a,clear}$ is the clear sky emissivity, proportional to $T_a{}^2$, and f_{cloud} the cloud cover fraction (Campbell and Norman, 1998).

The expansion on the far r.h.s. of Eq. (S4) is based on the linearization of the canopy emittance term, exploiting the binomial expansion. There, $B_{n,ref}^{\downarrow}$ is the net isothermal longwave energy absorbed by the canopy (subscript *ref*) and $\Delta B^{\downarrow}$ is the deviation from that. They were calculated as

$$\begin{aligned} B_{n,ref}^{\downarrow} &= \big(\varepsilon_a \sigma T_a^4 - \varepsilon_c \sigma T_a^4\big)\big[1 - exp\big(-K_{bl,d}\ L_{AI}\big)\big] \\ \Delta B^{\downarrow} &= 4\ \varepsilon_c \sigma T_a^3\ (T_a - T_c)\big[1 - exp\big(-K_{bl,d}\ L_{AI}\big)\big] \end{aligned}. \tag{S5}$$

S1.1.2 Wind velocity

To determine the wind velocity at the canopy height, h_c, $U(h_c)$, we considered the atmospheric bulk wind velocity and assumed a logarithmic wind profile above the canopy, including the diabatic corrections, i.e.,

$$U(z) = \frac{u^*}{K_v}\left[ln\left(\frac{z - d_0}{z_M}\right) + \Psi_M\right] \tag{S6}$$

Here, z is the generic height above the ground (set to h_c to determine $U(h_c)$), u^* the friction velocity, K_v the von Karman constant, d_0 the zero plane displacement ($d_0 \cong 2/3\ h_c$), z_M the roughness length for the momentum, and Ψ_M the diabatic correction factor for momentum. The diabatic correction factor was determined based on the following empirical functions, for unstable ($H \geq 0$, with H being the sensible heat flux; Eq. S20 below) and stable ($H < 0$) conditions (Campbell and Norman, 1998):

$$\Psi_M = \begin{cases} -1.2\ ln\left[\frac{1+(1-16\zeta)^{1/2}}{2}\right] & H \geq 0 \\ 6\ ln(1 + \zeta) & H < 0 \end{cases}. \tag{S7}$$

ζ is the atmospheric stability, accounting for the effects of buoyancy, measured as the ratio of the convective to mechanical production of turbulence (Bonan, 2019)

$$\zeta = -\frac{K_v g (z - d_0) H}{\hat{\rho}_a c_p T_a u^{*3}}, \qquad (S8)$$

where K_v is the von Karman constant, g the gravitational acceleration, z the height from the ground, $\hat{\rho}_a$ the molar density of air, c_p the heat capacity of air, T_a the air temperature at height z (expressed in Kelvin), and u^* the friction velocity. The latter was obtained by rearranging the diabatic profile equation for wind velocity at height z, $U(z)$, to yield $u^* = K_v U(z) \left[ln \left(\frac{z - d_0}{z_M} \right) + \Psi_M \right]^{-1}$.

S1.1.3 Vapor pressure deficit and air CO₂ concentration

It was assumed that turbulent transport is such that the relative humidity and the air CO_2 concentration at the canopy level are the same as the reference ones, well above the canopy.

S1.2 CO₂, water vapor and heat canopy exchanges

S1.2.1 CO₂ assimilation and stomatal conductance

The stomatal conductance g_s was modeled based on the optimization principle, i.e., assuming that plants maximize cumulated net CO_2 uptake over a given period, subject to limited water availability. The optimization principle and the optimal control theory provide the necessary condition for the stomatal conductance g_s to be optimal as $\partial(A_{net} - \lambda_w E_l)/\partial g_s = 0$ (Mäkelä et al., 1996), where $\lambda_w = \partial A_{net} / \partial E_l$ is the marginal water use efficiency, A_{net} is the net CO_2 assimilation rate, and E_l is the transpiration rate (both expressed on a per unit leaf area basis).

In contrast to other optimization models based on water use efficiency (Katul et al., 2009; Medlyn et al., 2011), here no *a priori* assumption was made on whether photosynthesis is light- or RuBisCO- limited. Rather, the Farquhar model of photosynthesis (Farquhar et al., 1980) was approximated by a hyperbolic function, as (Vico et al., 2013)

$$A_{net} = k_1 \frac{c_i - \Gamma^*}{k_2 + c_i} - R_d, \qquad (S9)$$

where c_i is the CO_2 concentration at the photosynthetic site (neglecting the mesophyll resistance), Γ^* is the CO_2 compensation point in the absence of dark respiration, R_d is the respiration rate in the light. The parameters k_1 and k_2 are related to the photosynthetic parameters as

$$k_1 = \frac{J}{4}$$

$$k_2 = \frac{J}{4} \frac{a_2}{V_{c,max}}. \qquad (S10)$$

Here, J is the electron transport rate, $V_{c,max}$ the maximum carboxylation rate; and $a_2 = K_C(1 + c_{Oa}/K_O)$, with K_C and K_O being the Michelis-Menten constants for CO_2 fixation and oxygen inhibition, and c_{Oa} the oxygen concentration in the air. The electron transport rate J depends on the light-saturated electron transport rate, J_{max}, and the available photosynthetically active radiation, expressed in µmol m⁻² s⁻¹ (obtained from $Q_{PAR}^{\downarrow}$ - Eq. S1-S3, assuming a constant conversion factor of 4.6 µmol J⁻¹).

The kinetic parameters (J_{max}, $V_{c,max}$, Γ^*, K_C and K_O) are a function of both canopy temperature (Bernacchi et al., 2001; Medlyn et al., 2002) and water availability (Vico and Porporato, 2008). The day respiration rate, R_d, was assumed to equal a fraction f_R of $V_{c,max}$, thus also depending on canopy temperature (and water availability).

85 The effects of water availability were considered directly on λ_w, $V_{c,max}$ and J_{max}. Following Zhou et al. (2013) and Manzoni et al. (2011), λ_w was assumed to be a function of the predawn canopy water potential $\psi_{c,pd}$ (set equal to the predawn soil water potential). Considering the predawn canopy water potential as opposed to the instantaneous one was motivated by λ_w not responding instantaneously to canopy water potential. A monotonically-increasing dependence on water availability was used to minimize the data needed for a robust relationship (Manzoni et al., 2011):

$$\lambda_w = \lambda_{ww}^* \frac{c_a}{c_a^*} exp(\beta_o \psi_{c,pd}), \tag{S11}$$

90 where λ_{ww}^* is the marginal water use efficiency under well-watered conditions and at reference atmospheric CO_2 concentration (c_a^*) and β_o is a fitting parameter describing the change in λ_w with water stress. More complex relationships have been suggested to match some observations, but they differ markedly only under extreme water stress (Manzoni et al., 2011) – conditions that are uncommon in most agricultural settings.

The effects of canopy water potential, ψ_c, on $V_{c,max}$ and J_{max} were accounted for via a Weibull-type vulnerability curve, the 95 parameters of which were determined by fitting physiological observations (Vico and Porporato, 2008). This approach allows accounting for non-stomatal limitations to photosynthesis under water stress – a mechanism necessary to reproduce observations (Zhou et al., 2013; Drake et al., 2017).

For simplicity, canopy water potential and temperature were not included in the optimization directly, but they did affect $V_{c,max}$, J_{max} and λ_w. This is equivalent to assuming that the marginal effect of g_s on T_c and ψ_c is small with respect to 100 that of g_s on A_{net} and E_l. It is important to emphasize that these assumptions apply only to the determination of stomatal conductance, i.e., all other modules include explicitly the roles of T_c and ψ_c.

This stomatal model represents a further development of that of Vico et al. (2013), because it explicitly includes the effects of water availability and day respiration, as well as the conductances to leaf boundary layer, and turbulent transport of vapor and heat, for more realistic estimates also under water stress and low wind velocity. The leaf boundary layer and turbulent transport 105 in the atmosphere can act as further resistances to the vapor and CO_2 exchanges with the surrounding atmosphere and decrease with wind velocity (see Eq. S13 below). Despite the additional feedbacks included in the model, a closed formula for the optimal stomatal conductance g_s can still be obtained, but it is cumbersome and hence not reported here.

S1.2.2 Minimum leaf conductance

In parallel to the stomatal conductance, we considered a minimum conductance, g_{min}, that cannot be controlled by the plant 110 (Kerstiens, 1996). g_{min} is known to change with water availability, although in ways that are complex, species-specific and not fully characterized yet (Duursma et al., 2019). And, while most of the experimental work has focused on the acclimation of g_{min} to low water availability as opposed to its instantaneous response, responses can occur even over few days (Bengtson et al., 1978). As a first approximation, it was assumed that g_{min} declines linearly with ψ_c, as

$$g_{min} = g_{min,ww} max\left(1 - \frac{\psi_c}{\psi_{c,0}}, 0\right) \tag{S12}$$

where $g_{min,ww}$ is the minimum conductance under well-watered conditions ($\psi_c = 0$) and $\psi_{c,0}$ is the leaf water potential at which the minimum conductance becomes negligible. Given the typically low value of $g_{min,ww}$, the exact functional dependence of g_{min} on ψ_c and its parameterization bears little consequences on the model outputs. Also, the role of g_{min} is negligible except under severe water stress, which, however, seldom occurs in most agricultural settings. Its inclusion was motivated to ensure that the model does not return unrealistic results should soil moisture reach an occasional low value during a prolonged dry down.

While g_{min} affects the amount of water lost by the leaves, it cannot be controlled by the plant and is independent of the stomatal conductance. So, considering in the optimization the total water losses at the leaf level, E_l, as opposed to the part stemming from the stomatal aperture only does not bear any consequence in the resulting optimized stomatal conductance.

S1.2.3 Canopy boundary layer conductances

The leaf boundary layer conductances to heat and vapor per unit leaf area ($g_{H,bl}$ and $g_{v,bl}$ respectively) were quantified as (Campbell and Norman, 1998):

$$g_{H,bl} = 1.4 \cdot 0.135 \sqrt{\frac{U(h_c)}{0.7 \, d_l}},$$

$$g_{v,bl} = 1.4 \cdot 0.147 \sqrt{\frac{U(h_c)}{0.7 \, d_l}}, \tag{S13}$$

where d_l is the leaf width (in m; and the coefficient 0.7 transforms it in the leaf characteristic dimension) and $U(h_c)$ is the wind velocity at canopy height (in m s^{-1}; Eq. S6).

S1.2.4 Aerodynamic bulk conductance

A further conductance, the aerodynamic bulk conductance (per unit ground area), $g_{H,a}$, is needed to describe the turbulent transport of heat and mass from outside the leaf boundary layer to the bulk atmosphere. This conductance was determined as (Webber et al., 2016; Campbell and Norman, 1998)

$$g_{H,a} = \frac{K_v^2 \hat{\rho}_a U(z)}{\left[ln\left(\frac{z-d_0}{z_M}\right) + \Psi_M\right]\left[ln\left(\frac{z-d_0}{z_H}\right) + \Psi_H\right]}, \tag{S14}$$

where z_i is the roughness length for momentum (for i=M) and heat (for i=H), and Ψ_i is the diabatic correction factor for momentum (i=M) and heat (i=H). The diabatic correction factor for momentum is given in Eq. (S7). From that, the diabatic correction factor for heat can be determined as (Campbell and Norman, 1998)

$$\Psi_H = \begin{cases} \frac{\Psi_M}{0.6} & H \geq 0 \\ \Psi_M & H < 0 \end{cases}. \tag{S15}$$

S1.2.5 Total canopy conductances

The total canopy conductance to water vapor (per unit ground area) was calculated as the series of stomatal and cuticular conductance, leaf boundary layer conductance, and aerodynamic bulk conductance. The minimum and stomatal conductance were assumed to operate in parallel, so that the net conductance is $g_{sc} = g_{min} + g_s$ and it converges to g_{min} during drought (as suggested by Duursma et al., 2019). This net conductance occurs in series with the leaf boundary layer conductance.

140   Assuming that both the abaxial and adaxial side of the leaf transpire at the same rate, the total leaf-level conductance to vapor per unit leaf area is

$$g_{v,l} = \frac{g_{sc}\, g_{v,bl}}{g_{sc} + g_{v,bl}} \tag{S16}$$

The total conductance to water vapor (per unit ground area), $g_{v,c}$, is given by the series of the leaf-level conductance, and aerodynamic conductance, $g_{H,a}$,

$$g_{v,c} = \frac{L_{AI} g_{v,l}\, g_{H,a}}{L_{AI} g_{v,l} + g_{H,a}} \tag{S17}$$

where the L_{AI} scales up the leaf level conductances to the canopy, exploiting the big-leaf approximation.

145   The total canopy conductance to heat (per unit ground area), $g_{H,c}$, is instead the series of the leaf boundary layer and aerodynamic bulk conductances, i.e.,

$$g_{H,c} = \frac{L_{AI} g_{H,bl}\, g_{H,a}}{L_{AI} g_{H,bl} + g_{H,a}} \tag{S18}$$

S1.2.6 Canopy energy balance

The canopy energy balance can be written as (Campbell and Norman, 1998)

$$Q^{\downarrow} + B_n^{\downarrow} = H + \lambda ET, \tag{S19}$$

where $Q^{\downarrow}$ and $B_n^{\downarrow}$ are the net incoming short- and long-wave radiations respectively, H is the sensible heat loss, and λET is the

150   latent heat loss, with ET being the transpiration rate (per unit ground area) and λ the latent heat of vaporization for water. The sensible heat loss depends on the temperature difference between the canopy and the air as

$$H = c_p g_{H,c}\, (T_c - T_a), \tag{S20}$$

The canopy transpiration rate (per unit ground area), ET, is given by

$$ET = g_{v,c} \frac{e_s(T_c) - e_a(T_a)}{P_a} \cong g_{v,c} s_s (T_c - T_a) + g_{v,c} D \tag{S21}$$

where $e_s(T_c)$ is the saturated vapor pressure at canopy temperature, $e_a(T_a)$ is the air vapor pressure, $s_s = \Delta\, P_a^{-1}$, with Δ being the slope of the saturation vapor pressure versus temperature function and P_a (kPa) the atmospheric pressure (Campbell and

155   Norman, 1998), and D is the air vapor pressure deficit. The expression on the far r.h.s. was obtained exploiting Penman's linearization of the saturated vapor pressure curve and it is line with the use of Penman Monteith equation for the calculation of canopy temperature.

Substituting Eq. (S4), (S20) and (S21) in Eq. (S19), the canopy energy balance reads

$$Q_{PAR}^{\downarrow} + Q_{NIR}^{\downarrow} + B_{n,ref}^{\downarrow} + \Delta B^{\downarrow} = c_p g_{H,c}(T_c - T_a) + \lambda g_{v,c} s_s(T_c - T_a) + \lambda g_{vc} D, \tag{S22}$$

where $Q_{NIR}^{\downarrow}$ and $Q_{NIR}^{\downarrow}$ were obtained via Eq. (S1). Rearranging the terms, the canopy temperature T_c was obtained explicitly as

$$T_c = T_a + \frac{Q_{PAR}^{\downarrow} + Q_{NIR}^{\downarrow} + B_{n,ref}^{\downarrow} - \lambda g_{v,c} D}{c_p g_{H,c} + \lambda g_{v,c} s_s + 4 \, \varepsilon_c \sigma T_a^3 \left[1 - exp(-K_{bl,d} \, L_{AI})\right]}. \tag{S23}$$

S1.3 Soil water balance and water transport along the soil-plant-atmosphere continuum (SPAC)

S1.3.1 Soil water balance

To limit parameter and computational requirements, we characterized plant available water by the soil water potential, averaged over the rooting depth, ψ_s, i.e., we neglected any potential inhomogeneity in root and soil water distribution in the soil volume where most of the plant roots are located. In turn, ψ_s is linked to the soil moisture, s (ranging from 0 for oven dry soils to 1 for saturated soils) as (Clapp and Hornberger, 1978)

$$\psi_s = \psi_{s,sat} \, s^{-b}, \tag{S24}$$

where $\psi_{s,sat}$ is the soil water potential at air entry and b is an empirical exponent. Both parameters depend on soil texture.

The most effective way to determine the dynamics of the soil moisture is via the soil water balance over the active rooting zone, of depth Z_r (Rodriguez-Iturbe et al., 1999; Vico and Porporato, 2011):

$$nZ_r \frac{ds}{dt} = P + I - ET_d - LQ, \tag{S25}$$

where s is the soil moisture, P is the input via (effective) precipitation, I is the irrigation, if any, ET_d is the cumulated daily losses via evapotranspiration, and the term LQ combines losses via surface runoff and percolation below the rooting zone. This balance is to be interpreted at the daily time scale, so that inputs and outputs are idealized as occurring instantaneously in time. The dependence on time of the terms in Eq. (S25) is not explicitly indicated for notational clarity.

Irrigation, if any, was assumed to be demand-based, i.e., irrigation is applied when soil moisture reaches a pre-set level (the intervention point, $\tilde{s}$). Each irrigation application provides a fixed amount of water, depending on the irrigation technology employed, equal to $nZ_r(\hat{s} - \tilde{s})$, where $\hat{s}$ is the level of moisture restored by each irrigation application (target level) (Vico and Porporato, 2011). The soil moisture intervention point and target level were set to corresponds to specific soil water potentials (as per Eq. S24), $\tilde{\psi}_s$ and $\hat{\psi}_s$ respectively, thus considering the effect of soil texture.

The loss via evapotranspiration was assumed to be dominated by losses via transpiration, in line with the focus on the anthesis phase, when canopies are closed and soil water evaporation becomes negligible (Wei et al., 2017). The cumulated daily losses via evapotranspiration was thus determined by cumulating the losses via canopy transpiration, ET (Eq. S21), during the day. The model was run only once per day, under the conditions likely resulting in the highest canopy temperatures (see Section 2.2 in the main text). To scale up losses via evapotranspiration at the daily scale, the daily evapotranspiration rate was assumed to follow a parabolic diurnal evolution. Hence, the total daily loss via evapotranspiration was determined as

$$ET_d = \frac{2}{3} ET \, (t_{sunset} - t_{sunrise}), \tag{S26}$$

where $t_{sunset} - t_{sunrise}$ is the day length, i.e., the time between sunrise and sunset.

185   Finally, in line with the daily interpretation of the water balance in Eq. (S25), losses via surface runoff and deep percolation below to the rooting zone, LQ, were assumed to occur instantaneously when soil moisture exceeds a threshold s_1, slightly above the soil field capacity. Hence, soil moisture dynamics is effectively upper-bounded by s_1.

S1.3.2 Soil-plant-atmosphere continuum

    The soil water balance was coupled to a minimalist description of the soil-plant-atmosphere continuum (SPAC), to determine
190   the leaf water potential. Water moves along the SPAC as driven by gradients of total water potential, from the soil to the leaf, and then to the atmosphere. Based on the electric analogy, the water flow was modulated by a series of resistances (or conductances): soil to root conductance; root to leaf (i.e., xylem) conductance; and leaf to the atmosphere (i.e., stomatal conductance). These conductances depend on soil features and plant traits, and decline with decreasing water potential. Details on these dependencies and parameter values are summarized in Manzoni et al. (2013).

195

S1.4 Environmental conditions above the canopy

    The model requires solar radiation, air temperature and humidity in the bulk atmosphere, at height $z > h_c$, as well as the daily precipitation totals. To explore different climatic scenarios, these environmental conditions were synthetically generated, as described next.

200   ### S1.4.1 Solar radiation

    The total incoming shortwave solar radiation, $Q_0^\downarrow$, was set to a realistic and constant value. Clear sky conditions were assumed for the entire anthesis, thus likely leading to an overestimate of T_c and a conservative estimate of the potential for heat damage.

S1.4.2 Precipitation

    Daily precipitation was idealized as a marked Poisson process, i.e., with exponentially distributed interarrival times,
205   τ_p (Rodriguez-Iturbe et al., 1999):

$$p_{\tau_p}(\tau_p) = \lambda_p\, e^{-\lambda_p\,\tau_p}\,, \quad \tau_p \geq 0, \tag{S27}$$

where λ_p is the average frequency of precipitation occurrence.

Each precipitation was assumed to occur instantaneously at the daily time scale (i.e., the temporal structure of precipitation is ignored). Each event provides a random amount h_p, assumed to be exponentially distributed

$$p_{h_p}(h_p) = \frac{1}{\alpha_p}\, e^{-\frac{1}{\alpha_p}h_p}\,, \quad h_p \geq 0, \tag{S28}$$

with α_p corresponding to the average precipitation depth.

210   With this model of precipitation, the average annual precipitation is $365\alpha_p\lambda_p$.

S1.4.3 Air temperature

    Since the focus was on the warmest part of the day, we interpreted T_a as the daily maximum temperature. The day-to-day fluctuations of T_a were described as an Ornstein-Uhlenbeck process (Benth and Benth, 2007). The rate of air temperature change was thus expressed as

$$\frac{dT_a}{dt} = -\frac{1}{\tau_{T_a}}\left(T_a - \mu_{T_a}\right) + \sqrt{k_3}\eta_t \qquad\qquad (S29)$$

where τ_{T_a} is the relaxation time (i.e., $\tau_{T_a}^{-1}$ is the mean-reversion rate of the process); μ_{T_a} is the long-term mean of maximum daily temperatures; k_3 is the diffusion parameter, quantifying the noise 'size'; and η_t is a Gaussian white noise (with vanishing mean, unit variance and an autocorrelation with a sharp peak in zero and dropping to zero for any lag greater than 0; Ridolfi et al., 2011). With these assumptions, T_a has a Gaussian distribution, with mean μ_{T_a} and standard deviation $\left(\frac{\tau_{T_a}k_3}{2}\right)^{1/2}$.

S1.4.4 Wind velocity and relative humidity

Wind velocity and relative humidity above the canopy were assumed to be constant during the simulation.

S1.5 Numerical simulations

For each climate and irrigation scenario and soil type, we run 501 simulations, each lasting 21 days (the duration of the heading period under current climatic conditions; Mäkinen et al., 2018). The initial conditions for soil water content and air temperature for each 21-day simulation correspond to the final conditions for the previous 21-day simulation, and hence are random. For the first simulation, the initial soil water potential was set at $\hat{\psi}_s$ and initial air temperature at μ_{T_a}, but this simulation was excluded to limit the influence of these arbitrary choices.

The model was solved via nested numerical iterations (Fig. 1 in the main text). For each day, air temperature and precipitation inputs were generated as detailed in Section S1.4. The T_c at the previous time step was used to determine the diabatic corrections and hence the aerodynamic conductance and the wind velocity, while ψ_c at the previous time step was used to estimate the aerodynamic and boundary layer conductances, the soil-to-leaf and optimal stomatal conductances (Eq. S6-S8, S12-S18). Then, the resulting water demand (driven by g_s, T_c and ψ_s, and D) was compared with the water supply through the soil, root and plant (driven by the series of soil to root to plant conductances, and the difference in water potential between the soil and the canopy). The ψ_c for which supply equaled demand was calculated and used in the subsequent iteration, where the values of conductances were updated. Once convergence on ψ_c was reached (i.e., when the absolute difference in ψ_c between two subsequent steps was smaller than $\psi_{c,toler}$), the iterative loop on ψ_c was exited, and the g_s value corresponding to such ψ_c was used in the canopy energy balance, to obtain a new estimate of T_c. This cycle was repeated till convergence was reached also on T_c (with tolerance $T_{c,toler}$), unless a pre-set number of iterations Max_{iter} was reached.

Once T_c was determined, the mid-day losses via transpiration were calculated and scaled up to the daily level (Eq. S26), and the daily soil moisture balance was updated, including any input via precipitation or irrigation. The new soil moisture s was used as the basis to determine the soil water potential for the subsequent day.

Table S1. List of symbols

Variable	Description	Units
a_2	Combination of the Michelis Menten constants for CO_2 fixation and oxygen inhibition	μmol mol⁻¹
A_{net}	Net CO_2 assimilation rate	μmol m⁻² s⁻¹
b	Exponent of soil water retention curve	-
$B_n^\downarrow$	Net incoming longwave radiation	W m⁻²
$B_{n,ref}^\downarrow$	Net isothermal longwave energy absorbed by the canopy	W m⁻²
c_a^*	Reference CO_2 concentration in the bulk atmosphere	μmol mol⁻¹
c_i	CO_2 concentration at the photosynthetic site	μmol mol⁻¹
c_{Oa}	Oxygen concentration in the bulk atmosphere	mmol mol⁻¹
c_p	Heat capacity of air	J kg⁻¹ K⁻¹
d_0	Zero plane displacement	m
d_l	Leaf width	m
D	Vapor pressure deficit	mol mol⁻¹
$e_a(T_a)$	Air vapor pressure at air temperature T_a	mol m⁻² s⁻¹
$e_s(T_c)$	Saturation vapor pressure at canopy temperature T_c	mol m⁻² s⁻¹
ET	Instantaneous evapotranspiration rate per unit ground area	mol m⁻² s⁻¹
ET_d	Daily evapotranspiration rate per unit ground area	m s⁻¹
ET_l	Instantaneous evapotranspiration rate per unit leaf area	mol m⁻² s⁻¹
f_{cloud}	Cloud cover fraction	-
f_{NIR}	Fraction of total radiation in the NIR wavebands	-
f_{PAR}	Fraction of total radiation in the PAR wavebands	-
f_R	Ratio between R_d and $V_{c,max}$	-
g	Gravitational acceleration	m s⁻²
$g_{H,a}$	Aerodynamic bulk conductance (per unit ground area)	mol m⁻² s⁻¹
$g_{H,bl}$	Leaf boundary layer conductance to heat (per unit leaf area)	mol m⁻² s⁻¹
$g_{H,c}$	Total canopy conductance to heat (per unit ground area)	mol m⁻² s⁻¹
g_{min}	Minimum conductance (cannot be controlled by the plant; per unit leaf area)	mol m⁻² s⁻¹
$g_{min,ww}$	Minimum conductance under well-water condition (per unit leaf area)	mol m⁻² s⁻¹
g_s	Stomatal conductance (per unit leaf area)	mol m⁻² s⁻¹
g_{sc}	Sum of stomatal and minimum conductance (per unit leaf area)	mol m⁻² s⁻¹
$g_{v,c}$	Total canopy conductance to water vapor (per ground area)	mol m⁻² s⁻¹
$g_{v,bl}$	Leaf boundary layer conductance to water vapor (per unit leaf area)	mol m⁻² s⁻¹
$g_{v,l}$	Leaf-level conductance to water vapor (per unit leaf area)	mol m⁻² s⁻¹
$G_{S,ref}$	Reference surface conductance rate	mmol · m⁻² · s⁻¹
G_s	Surface conductance (per unit ground area)	mmol · m⁻² · s⁻¹

h_c	Canopy height	m
h_p	Precipitation event depth	m
H	Sensible heat flux	W m^{-2}
I	Irrigation application	m d^{-1}
J	Electron transport rate	µmol m^{-2} s^{-1}
J_{max} ($J_{max,25}$)	Maximum electron transport rate (and reference value at 25 °C)	µmol m^{-2} s^{-1}
k_1	Parameter of the hyperbolic photosynthetic model (Eq. (S10))	µmol m^{-2} s^{-1}
k_2	Parameter of the hyperbolic photosynthetic model (Eq. (S10))	µmol mol^{-1}
k_3	Diffusion parameter of air temperature (noise 'size')	°C^2 d^{-1}
K_{bl}	Extinction coefficient for black leaves	-
$K_{bl,d}$	Extinction coefficient for black leaves, under diffuse light and longwave radiation	-
K_C	Michelis-Menten constants for CO$_2$ fixation	µmol mol^{-1}
K_O	Michelis-Menten constants for oxygen inhibition	mmol mol^{-1}
K_{sat}	Soil hydraulic conductivity at saturation	m d^{-1}
K_v	Von Karman constant	-
L_{AI}	Leaf area index	m^2 m^{-2}
LQ	Surface runoff and deep percolation below the rooting depth	m d^{-1}
m	Slope of surface conductance to water pressure deficit	[ln(kPa)]$^{-1}$
Max_{iter}	Maximum iteration number	-
n	Soil porosity	-
P	Daily total precipitation	m d^{-1}
P_a	Air pressure	kPa
P_{CHS}	Fraction of days during which T_c exceeded T_{th}	-
$Q^{\downarrow}$	Total net shortwave radiation absorbed by the canopy	W m^{-2}
$Q^{\downarrow}_{0,i}$	Solar radiation above the canopy (i= NIR, PAR)	W m^{-2}
$Q^{\downarrow}_{i}$	Total radiation of the component (i= NIR, PAR)	W m^{-2}
R_d	Respiration rate in the light	µmol m^{-2} s^{-1}
RH	Air relative air humidity	-
s	Soil moisture	-
s_s	Slope of the vapor pressure vs. temperature curve	kPa K^{-1}
s_1	Soil moisture above which runoff and percolation below the active rooting zone occur instantaneously	-
t	Time	d
$t_{sunrise}, t_{sunset}$	Time of sunrise, time of sunset	hr
T_a	Air temperature	°C
T_c	Canopy temperature	°C
$T_{c,toler}$	Canopy temperature tolerance	°C

Symbol	Description	Units
T_{th}	Threshold above which crop heat stress occurs around anthesis period	°C
u^*	Friction velocity	m s^{-1}
$U(z)$	Mean wind velocity at height z	m s^{-1}
$V_{c,max}$ ($V_{c,max,25}$)	Maximum carboxylation rate (and reference value at 25 °C)	μmol $\cdot$ m^{-2} $\cdot$ s^{-1}
z	Height from the ground	m
z_M	Roughness length for the momentum	m
z_U	Height of wind measurement	m
Z_r	Active rooting depth	m
α_p	Average precipitation event depth	m
β_o	Fitting parameter of the marginal water use efficient response function to water stress	-
Γ^*	CO_2 compensation point in the absence of dark respiration	mol mol^{-1}
Δ	Slope of the vapor pressure vs. temperature curve	mol mol^{-1} K^{-1}
$\Delta B^{\downarrow}$	Deviation of absorbed energy	W m^{-2}
ε_a	Apparent longwave emissivity for a hemisphere radiating at temperature T_a	-
$\varepsilon_{a,clear}$	Clear sky emissivity	-
ε_c	Longwave canopy emissivity	-
ζ	Atmospheric stability	-
θ_{sun}	Solar zenith angle	rad
λ	Latent heat of vaporization for water	J kg^{-1}
λ_p	Average precipitation frequency	day^{-1}
λ_w	Marginal water use efficiency	mol mol^{-1}
λ_{ww}^*	Marginal water use efficiency under well-watered condition and reference air CO_2 concentration	mol mol^{-1}
μ_{T_a}	Long-term mean air temperature	°C
$\hat{\rho}_a$	Molar density of air	mol m^{-3}
ρ_i	Canopy reflection coefficient for PAR (i=PAR) and NIR (i=NIR)	-
σ	Stefan-Boltzman constant	W m^{-2} K^{-4}
σ_i	Leaf scattering coefficient for PAR (i=PAR) and NIR (i=NIR)	-
τ_p	Precipitation interarrival time	d
τ_{T_a}	Relaxation time (i.e., $\tau_{T_a}^{-1}$ is the mean-reversion rate of the Ornstein-Uhlenbeck process)	d
$\psi_{c,0}$	Leaf water potential at which minimum conductance becomes negligible	MPa
ψ_c	Canopy water potential	MPa
$\psi_{c,pd}$	Predawn canopy water potential	MPa
$\psi_{c,toler}$	Canopy water potential tolerance	MPa
ψ_s	Soil water potential	MPa

$\tilde{\psi}_s$	Irrigation intervention soil water potential	MPa
$\hat{\psi}_s$	Target soil water potential for irrigation	MPa
$\psi_{s,sat}$	Soil water potential at saturation	MPA
Ψ_i	Diabatic correction factor (i= H for heat; i=M for momentum)	MPa

Table S2. List of parameters

Symbol	Value	Unit	Source
Crop parameters			
C_d	0.3	-	(Katul et al., 2004; crop canopies)
d_0	2/3 h_c	m	(Jones, 1992)
d_l	0.04	m	
f_R	0.01	-	
$g_{min,ww}$	1.73×10^{-2}	$mmol \cdot m^{-2} \cdot s^{-1}$	(Duursma et al., 2019; mean value for wheat)
h_c	0.6	m	
$J_{max,25}$	132	$\mu mol \cdot m^{-2} \cdot s^{-1}$	(Wullschleger, 1993; wheat)
K_c	405	$\mu mol\ mol^{-1}$	
K_O	278	$mmol\ mol^{-1}$	
L_{AI}	2	$m_{leaf}^2\ m_{ground}^{-2}$	(Vico and Porporato, 2008)
T_{th}	30	°C	(Saini and Aspinall, 1982)
$V_{c,max,25}$	83	$\mu mol \cdot m^{-2} \cdot s^{-1}$	(Wullschleger, 1993; wheat)
Z_r	0.3	m	
β_o	-1.26	MPa^{-1}	(Manzoni et al., 2011; median value for forbs and grasses in mesic and wet climates)
λ_{ww}^*	981	$mol\ mol^{-1}$	(Manzoni et al., 2011; median value for forbs and grasses in mesic and wet climates)
$\psi_{c,0}$	-3	MPa	
Environmental conditions			
c_a^*	400	$\mu mol\ mol^{-1}$	
C_{Oa}	210	$mmol\ mol^{-1}$	
k_3	32.6	$°C^2\ d^{-1}$	(Rigby and Porporato, 2008)
RH	40%	-	
P_a	101	kPa	

$Q_0^\downarrow$	800	W m^{-2}	
$U(z_U)$	4	m s^{-1}	
z_M	0.13 h_c	m	(Jones, 1992)
z_U	2	m	
α_p	8.2	mm	Baseline scenario
λ_p	0.2	d^{-1}	Baseline scenario
μ_{T_a}	25	°C	Baseline scenario
τ_{T_a}	0.81	d	(Rigby and Porporato, 2008)
Soil parameters			
b	4.38 (loamy sand) 4.90 (sandy loam) 5.39 (loam)	-	(Laio et al., 2001)
n	0.42 (loamy sand) 0.43 (sandy loam) 0.45 (loam)	-	(Laio et al., 2001)
K_{sat}	1.0 (loamy sand) 0.8 (sandy loam) 0.2 (loam)	m d^{-1}	(Laio et al., 2001)
s_1	0.57 (sandy loam), 0.62 (loamy sand) 0.72 (loam)	-	(Laio et al., 2001)
$\tilde{\psi}_s$	-0.07	MPa	
$\hat{\psi}_s$	-0.01	MPa	
$\psi_{s,sat}$	-1.7×10^{-4} (loamy sand) -7×10^{-4} (sandy loam) -1.43×10^{-3} (loam)	MPa	(Laio et al., 2001)
Energy balance parameters			
f_{cloud}	0.1 (i.e., clear skies)	-	
f_{NIR}	0.55	-	(Campbell and Norman, 1998)

f_{PAR}	1-f_{NIR}	-	(Campbell and Norman, 1998)
$K_{bl,d}$	0.8	-	(Campbell and Norman, 1998)
$\varepsilon_{a,clear}$	$9.2 \ 10^{-6} T_a^2$	-	(Swinbank equation; Campbell and Norman, 1998)
ε_c	0.97	-	(Campbell and Norman, 1998)
ρ_i	0.057 (i=PAR) 0.389 (i=NIR)	-	(Leuning et al., 1995)
σ_i	0.2 (i=PAR) 0.8 (i=NIR)	-	(Leuning et al., 1995; Goudriaan and Van Laar, 1994)

Numerical simulation parameters

Max_{iter}	15	-	
$T_{c,toler}$	0.1	°C	
$\psi_{c,toler}$	0.001	MPa	

245

S2 Model behavior

The temporal evolution of key model variables during a soil moisture dry down, assuming constant air temperature at 25 °C, is presented in Fig. S1, and the dependences on soil moisture in Fig. S2. As soil moisture decreased, the canopy-to-air temperature difference $T_c - T_a$ and the marginal water use efficiency λ_w increased; while maximum carboxylation rate $V_{c,max}$, net CO_2 assimilation rate A_{net}, total leaf-level conductance to water vapor $g_{v,l}$ and the leaf, root and soil water potentials ψ_l, ψ_r and ψ_s rapidly became more negative. Conversely, all the variables were largely independent of soil moisture under well-watered conditions.
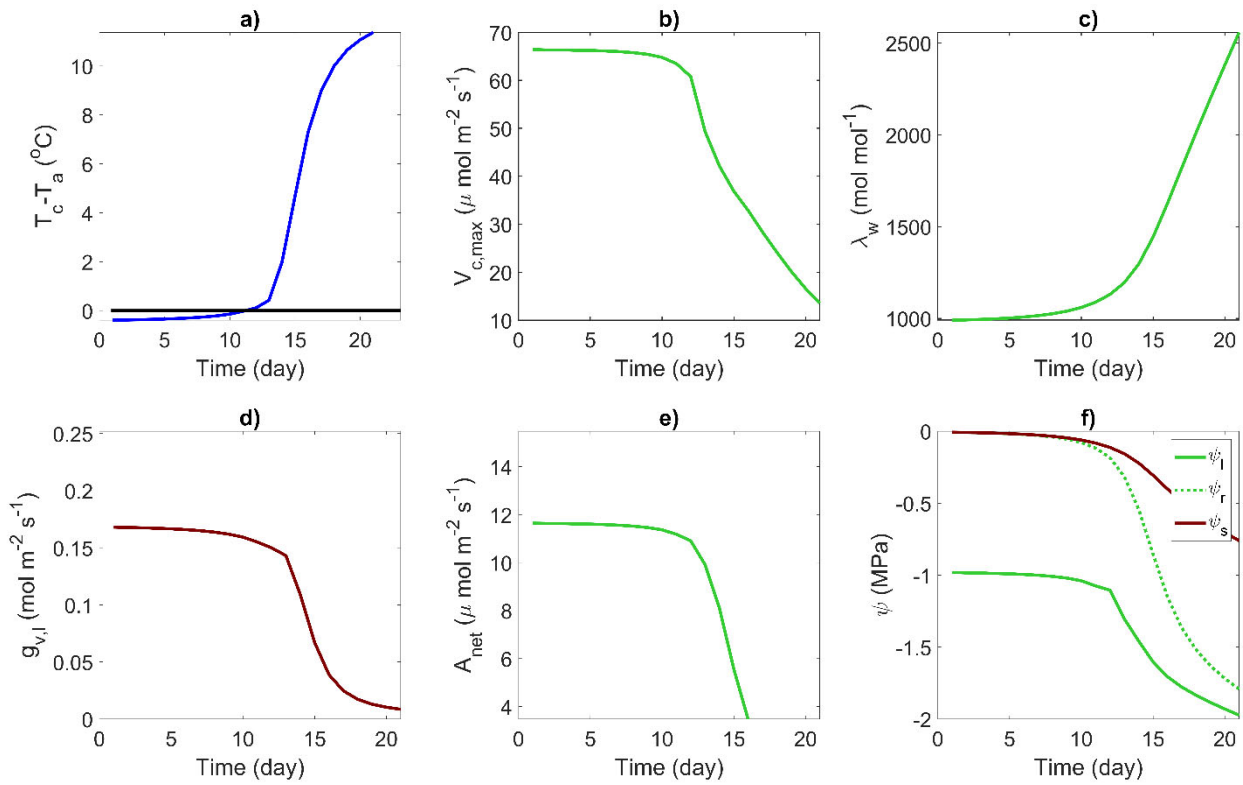
Figure S1. Temporal evolution of the key model variables during a dry down with $T_a = 25°C$: a) canopy temperature difference $T_c - T_a$, b) maximum carboxylation rate $V_{c,max}$, c) marginal water use efficiency λ_w, d) total leaf-level conductance to water vapor $g_{v,l}$, e) net CO_2 assimilation rate A_{net}, f) leaf, root, and soil water potentials, ψ_l, ψ_r and ψ_s.
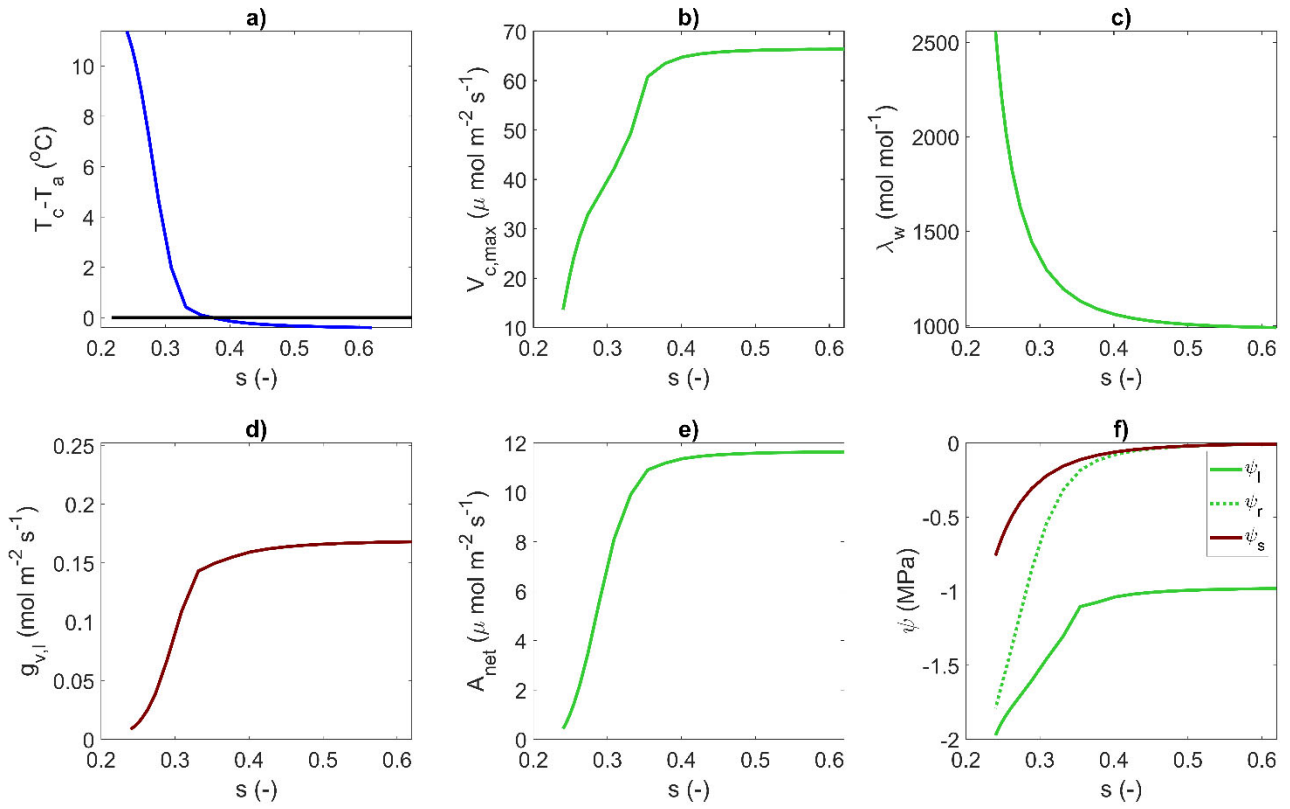
Figure S2. Dependence of the key variables on soil moisture s: a) canopy temperature difference $T_c - T_a$, b) maximum carboxylation rate $V_{c,max}$, c) marginal water use efficiency λ_w, d) total leaf-level conductance to water vapor $g_{v,l}$, e) net CO_2 assimilation rate A_{net}, f) leaf, root, and soil water potentials, ψ_l, ψ_r and ψ_s.

S3 Additional results

S3.1 Effects of air temperature variability

We tested different air temperature variability by altering the diffusion parameter (noise 'size') k_3, to which the air temperature variance is proportional. The pattern of T_c and P_{CHS} were independent of k_3 for rainfed conditions, but their medians and variance increased with increasing diffusion parameter under irrigation (Fig. S3, Table S7).
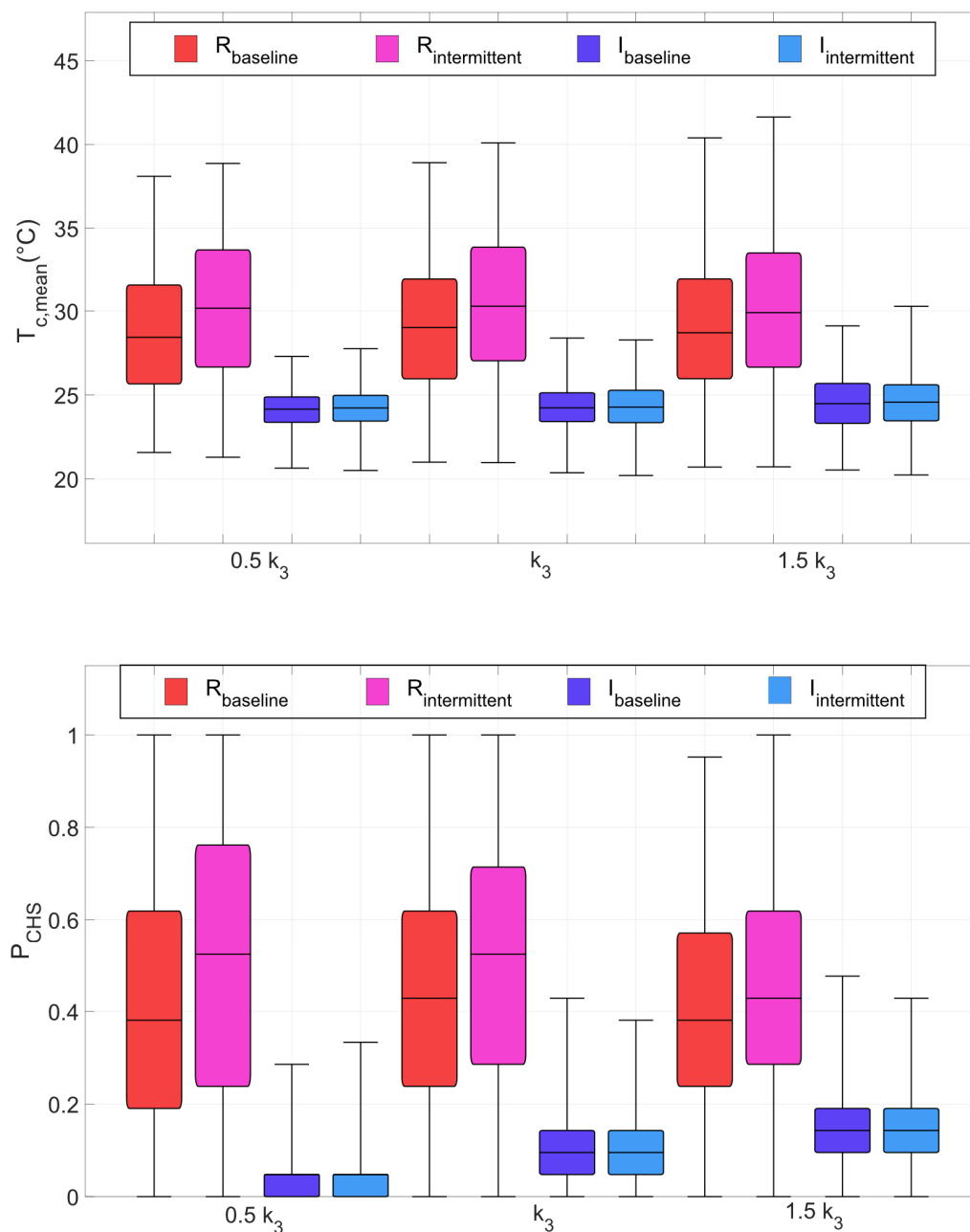
Figure S3. Mean canopy temperature during anthesis, $T_{c,mean}$ (top) and percentage of days during which $T_c > T_{th}$, P_{CHS} (bottom) under three noise 'sizes', corresponding to half of the baseline (left), baseline (center) and 1.5 times the baseline (right). Long-term mean air temperature was kept at μ_{T_a}=25 °C. R_baseline and R_intermittent represent rainfed cropping, under baseline precipitation (α_p =8.2 mm; λ_p =0.2 d⁻¹) and more intermittent precipitation (α_p =23.5 mm ; λ_p = 0.07 d⁻¹) respectively. I_baseline and I_intermittent refer to stress avoidance irrigation, under the same precipitation regimes as for the corresponding rainfed case. For each climatic scenario, 500 21-day simulations were run. The horizontal dark lines are the median values; the boxes extend from the first to the third quartile; whiskers cover the whole range.

S3.2 Effects of soil texture

Soil texture determines the soil water storage capacity, the losses below the rooting zone, and the ability of the plant to take up water. Despite these potential roles of soil texture on soil and water plant dynamics, soil texture had no effect on median and variance of $T_{c,mean}$ and P_{CHS}, although the differences induced by the precipitation regime remained (Fig. S4, Table S8).
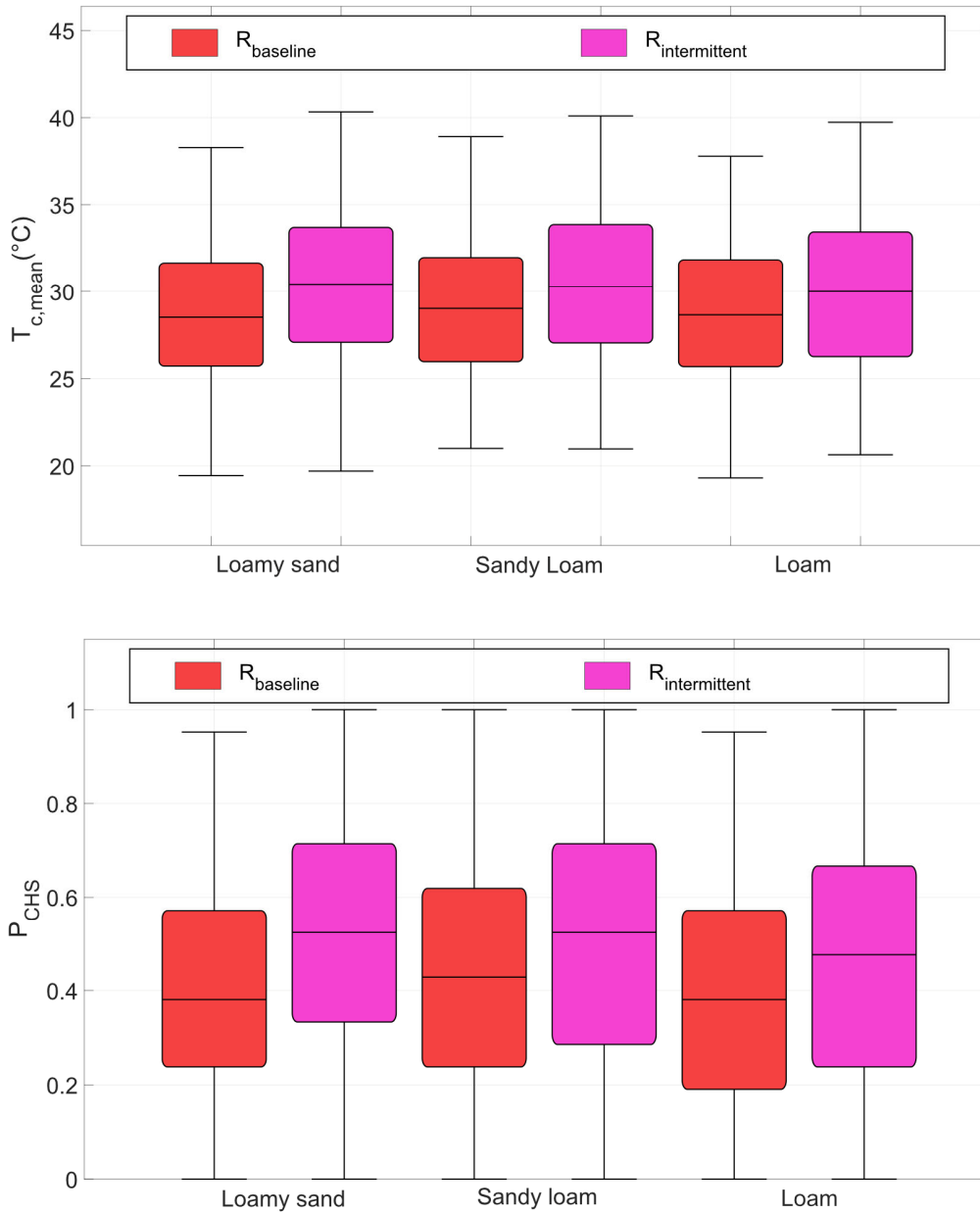
Figure S4. Mean canopy temperature during anthesis, $T_{c,mean}$ (top) and percentage of days during which $T_c > T_{th}$, P_{CHS} (bottom) for three soil types: from left to right, loamy sand (baseline), sandy loam, and loam. R_baseline and R_intermittent represent rainfed cropping, under baseline precipitation (α_p =8.2 mm ; λ_p =0.2 d^{-1}) and more intermittent precipitation (α_p =23.5 mm; λ_p = 0.07 d^{-1}) respectively. For each precipitation scenario and soil type, 500 21-day simulations were run. The horizontal dark lines are the median values; the boxes extend from the first to the third quartile; whiskers cover the whole range.

S3.3 Effects of solar radiation, wind velocity, and air relative humidity

We tested the sensitivity of T_c to radiation $Q_0^\downarrow$, wind velocity U, and relative humidity RH, at different soil moistures (Fig. S5).
290   Higher $Q_0^\downarrow$ led to higher T_c. Lower U enhanced canopy temperature at low soil moisture. High RH slightly increased T_c at high soil moisture.
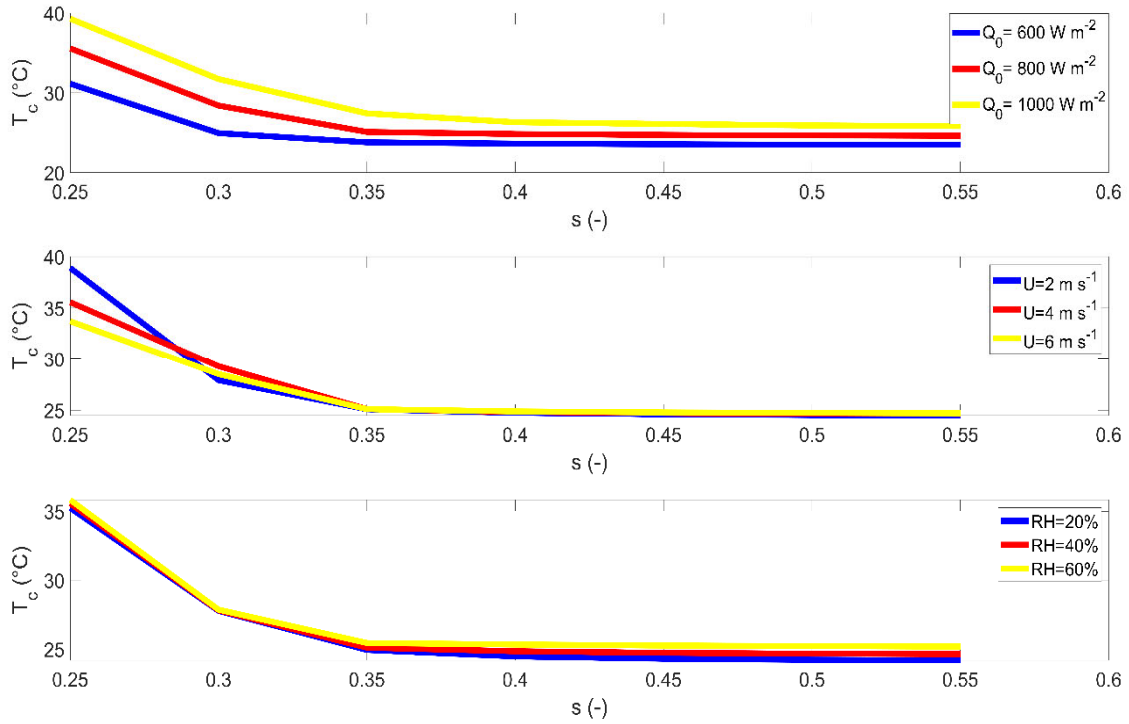
Figure S5. Canopy temperature, T_c, as a function of soil moisture, s, as obtained for three levels of short-wave radiations $Q_0^\downarrow$ (top), wind velocity U (center), and relative humidity RH (bottom). All the other parameters are as in Table S2.

295

S4 Statistical tests

We tested whether medians and variance of $T_{c,mean}$ and P_{CHS} differed between pedoclimatic scenarios, by means of Mood's

median test and Brown-Forsythe's test of equal variance. Results are summarized in Table S3 to S8.

Table S3. Statistical tests of the effects of average annual precipitation amount at different long-term mean air temperature, μ_{T_a} (columns), based on 500 simulations. For each test, the test statistics (top) and p value (bottom) are reported. The degrees of freedom (df) are specified for each type of test. Data are summarized in Fig. 4 in the main text.

		20 °C	25 °C	30 °C
$T_{c,mean}$	Test on equal median df=3	232.02 <0.001	228.78 <0.001	177.49 <0.001
	Test on equal variance df=[3, 1996]	42.36 <0.001	20.82 <0.001	7.97 <0.001

Table S4. Statistical tests of the effects long-term mean air temperatures for different average annual precipitation totals (from 500 to 1100 mm), based on 500 simulations. For each test, the test statistics (top) and p value (bottom) are reported. The degrees of freedom (df) are specified for each type of test. Data are summarized in Fig. 4 in the main text.

		500 mm	700 mm	900 mm	1100 mm
$T_{c,mean}$	Test on equal median df=2	562.80 <0.001	566.27 <0.001	692.50 <0.001	825.14 <0.001
	Test on equal variance df=[2,1497]	4.55 <0.05	12.87 <0.001	16.70 <0.001	47.43 <0.001

Table S5. Statistical tests of the effects of precipitation patterns and irrigation at different long-term mean air temperatures, based on 500 simulations. For each test, the test statistics (top) and p value (bottom) are reported. The degrees of freedom (df) are specified for each type of test. Data are summarized in Fig. 5 in the main text.

		20 °C				25 °C				30 °C			
		Effect of precipitation pattern		Effect of irrigation		Effect of precipitation pattern		Effect of irrigation		Effect of precipitation pattern		Effect of irrigation	
		Rainfed	Irrigated	Baseline precipitation	More intermittent precipitation	Rainfed	Irrigated	Baseline precipitation	More intermittent precipitation	Rainfed	Irrigated	Baseline precipitation	More intermittent precipitation
		$R_{baseline}$ vs $R_{intermittent}$	$I_{baseline}$ vs $I_{intermittent}$	$R_{baseline}$ vs $I_{baseline}$	$R_{intermittent}$ vs $I_{intermittent}$	$R_{baseline}$ vs $R_{intermittent}$	$I_{baseline}$ vs $I_{intermittent}$	$R_{baseline}$ vs $I_{baseline}$	$R_{intermittent}$ vs $I_{intermittent}$	$R_{baseline}$ vs $R_{intermittent}$	$I_{baseline}$ vs $I_{intermittent}$	$R_{baseline}$ vs $I_{baseline}$	$R_{intermittent}$ vs $I_{intermittent}$
$T_{c,mean}$	Test on equal median df=1	17.42 <0.001	3.14 0.08	138.38 <0.001	287.30 <0.001	12.54 <0.001	0.14 0.7	345.74 <0.001	484.42 <0.001	16.38 <0.001	0.78 0.38	484.42 <0.001	501.26 <0.001
	Test on equal variance df=[1,998]	13.32 <0.001	1.17 0.28	316.45 <0.001	478.06 <0.001	6.39 <0.05	1.39 0.24	468.75 <0.001	457.52 <0.001	4.11 <0.05	0.55 0.46	328.22 <0.001	417.16 <0.001
P_{CHS}	Test on equal median df=1	20.22 <0.001	1.34 0.25	302.94 <0.001	427.85 <0.001	22.03 <0.001	0.71 0.40	490.96 <0.001	521.10 <0.001	15.40 <0.001	0.90 0.34	472.21 <0.001	446.80 <0.001
	Test on equal variance df=[1,998]	16.45 <0.001	2.08 0.15	394.09 <0.001	723.33 <0.001	5.55 <0.05	0.19 0.67	536.66 <0.001	590.33 <0.001	0.84 0.36	0.04 0.84	116.85 <0.001	131.57 <0.001

Table S6. Statistical tests of the effects long-term mean air temperatures for different precipitation patterns and irrigation, based on 500 simulations. For each test, the test statistics (top) and p value (bottom) are reported. The degrees of freedom (df) are specified for each type of test. Data are summarized in Fig. 5 in the main text.

		Rainfed		Irrigated	
		Baseline precipitation	More intermittent precipitation	Baseline precipitation	More intermittent precipitation
$T_{c,mean}$	Test on equal median df=2	640.19 <0.001	534.35 <0.001	984.11 <0.001	1000 <0.001
	Test on equal variance df=[2,1497]	7.19 <0.001	2.55 0.08	8.18 <0.001	5.39 <0.01
P_{CHS}	Test on equal median df=2	571.54 <0.001	473.04 <0.001	924.70 <0.001	972.86 <0.001
	Test on equal variance df=[2,1497]	27.75 <0.001	19.92 <0.001	276.15 <0.001	292.53 <0.001

320

Table S7 Statistical tests of the role of air temperature variance on median and variance of canopy temperatures, for different rainfall patterns and management combinations, based on 500 simulations. For each test, the test statistics (top) and p value (bottom) are reported. The degrees of freedom (df) are specified for each type of test. Data are summarized in Fig. S3.

		Rainfed		Irrigated	
		Baseline precipitation	More intermittent precipitation	Baseline precipitation	More intermittent precipitation
$T_{c,mean}$	Test on equal median df=2	1.78 0.41	1.78 0.41	12.74 <0.01	8.26 <0.05
	Test on equal variance df=[2,1497]	0.09 0.91	0.24 0.79	33.61 <0.001	23.47 <0.001
P_{CHS}	Test on equal median df=2	4.52 0.10	7.62 <0.05	327.84 <0.001	295.51 <0.001
	Test on equal variance df=[2,1497]	19.31 <0.001	27.69 <0.001	68.09 <0.001	65.21 <0.001

Table S8. Statistical tests of the role of soil texture on canopy temperature mean and variance, based on 500 simulations. For each test, the test statistics (top) and p value (bottom) are reported. The degrees of freedom (df) are specified for each type of test. Data are summarized in Fig. S4.

325

		Baseline precipitation	More intermittent precipitation
$T_{c,mean}$	Test on equal median df=2	1.34 0.51	0.98 0.61
	Test on equal variance df=[2,1497]	0.20 0.82	0.46 0.63
P_{CHS}	Test on equal median df=2	2.73 0.26	2.42 0.30
	Test on equal variance df=[2,1497]	0.04 0.96	1.47 0.23

S5 Methodological considerations

S5.1 Modeling assumptions and their implications

The model developed does not explicitly take into account the vertical dimension, i.e., the canopy was approximated by a big leaf and the soil moisture balance was represented via a bucket-filling model.

The big-leaf approximation scales up the leaf-level carbon and water fluxes, assuming that the entire canopy is subject to the same conditions and behaves in the same way. Hence, sunlit and shaded leaves cannot be distinguished. This could underestimate the effects of solar radiation and the temperature of sunlit leaves. Indeed, T_c simulated by big-leaf model was around 1 °C higher than the simulated temperatures for shaded leaves but lower than those of sunlit leaves (Dai et al., 2004). Yet, we considered solar radiation at the top of the canopy, thus effectively representing sunlit leaves, i.e., providing an overestimate of the temperatures to which leaves are exposed. Further, the big-leaf approximation cannot capture the effects of the wind velocity profile within the canopy, leading to canopy layers nearer to the ground to be warmer than the higher ones. These are also the layers where solar radiation is lower, thus potentially balancing out the effects of the simplifications implicit in the big-leaf framework.

While the model is capable of simulating the diurnal cycle and the whole growing season, we limited the analyses to the warmest part of the day and the crop's most sensitive developmental stage, anthesis. Similarly, the model can accommodate the temporal evolution of environmental conditions beyond air temperature and precipitation occurrence, but we set them constant and interpreted them as averages (for RH and U) and maximum (for $Q_0^{\downarrow}$) during the simulation period. We also assumed clear skies, thus potentially overestimating canopy temperatures when compared with cloudy conditions. Taken together, these assumptions led to an overestimate of T_c and hence of the frequency of canopy temperature exceeding the threshold for potential damage.

S5.2 Alternative approach to estimating canopy conductance

The soil moisture – canopy conductance relation emerging from the stomatal optimization model coupled with the SPAC (Eq. S9-S18) was compared with an empirical model of canopy-level conductance determined based on eddy covariance data. The dependence of canopy conductance to water vapor on D was shown to be well approximated as (Oren et al., 1999):

$$G_s = G_{s,ref} \cdot [1 - m \cdot \ln(P_a\, D)], \tag{S30}$$

where P_a is the air pressure (in kPa); the intercept parameter $G_{S,ref}$ is the reference surface conductance rate (mmol m^{-2} s^{-1}) corresponding to the conductance at $D = 10^{-2}$ mol mol^{-1}; and the slope parameter m ($[ln(kPa)]^{-1}$) represents the sensitivity of surface conductance to D. Both $G_{S,ref}$ and m increase with soil water availability, as e.g. shown by a synthesis of eddy covariance data (Novick et al., 2016). For crops, a linear regression of the data presented by Novick et al. (2016) yielded

$$G_{s,ref} = 552\,\theta + 259, \tag{S31}$$

$$m = 0.57\,\theta + 0.13, \tag{S32}$$

where θ is the volumetric soil water content, related to the soil moisture s as $\theta = n\,s$, with n being the soil porosity.

During a dry down, the predicted surface conductance obtained with the empirical approach (Eq. S30-S32) and the mechanistic model used in this work (Eq. S9-S18) were similar at air temperature $T_a = 20$ °C, but the empirical model provided a higher

value of conductance at $T_a = 15$ °C and a lower one at $T_a = 25$ °C and 30 °C (Fig. S6). These discrepancies underline the importance of including mechanistically all the temperature dependences, unless site- and crop-specific data are available to correctly determine the canopy conductance empirically.
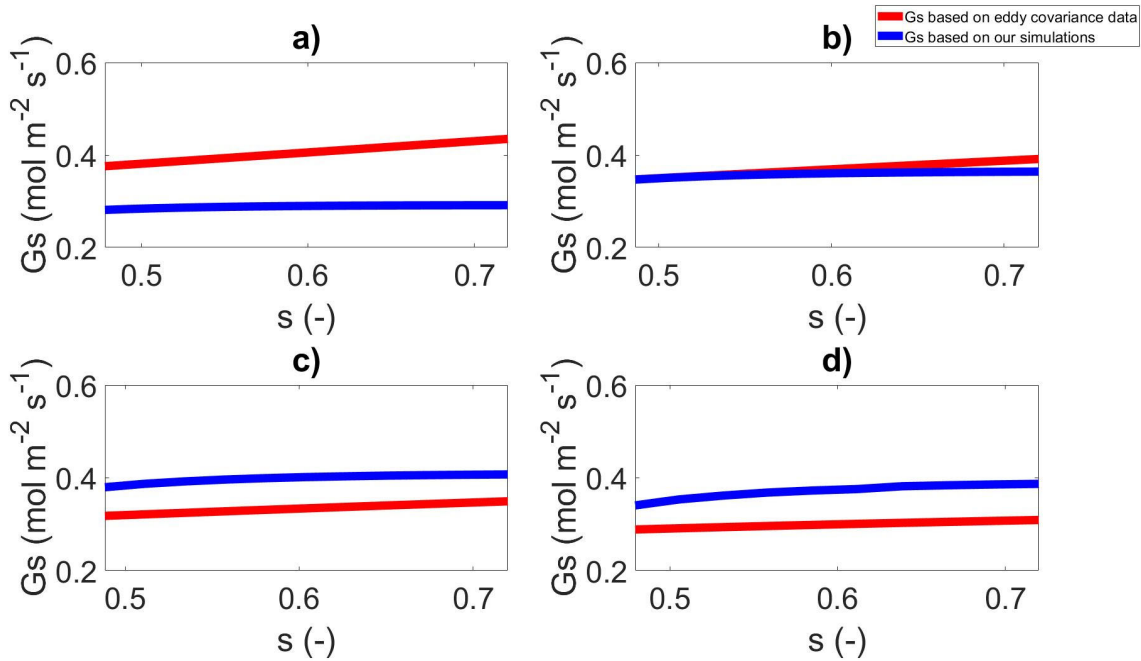
Figure S6. Comparison of two approaches to the determination of the canopy conductance for different air temperatures (a, b, c, d correspond to $T_a = 15, 20, 25, 30$ °C respectively). Surface conductance G_s (mol m^{-2} s^{-1}) as a function of soil moisture s, based on the upscaling of the leaf level optimal stomatal conductance (in blue) is compared with the empirical model based on eddy covariance data (Eq. S30-S32; in red). To avoid extrapolations, the range of soil moisture considered corresponds to that for which data on G_s are available in Novick et al. (2016).

References

Amthor, J. S.: Scaling CO$_2$-photosynthesis relationships from the leaf to the canopy, Photos Res, 39, 321-350, https://doi.org/10.1007/bf00014590, 1994.

Bengtson, C., Larsson, S., and Liljenberg, C.: Effects of water stress on cuticular transpiration rate and amount and composition of epicuticular wax in seedlings of six oat varieties, Physiol Plantarum, 44, 319-324, https://doi.org/10.1111/j.1399-3054.1978.tb01630.x, 1978.

Benth, F. E., and Benth, J. Š.: The volatility of temperature and pricing of weather derivatives, Quant Finance, 7, 553-561, https://doi.org/10.1080/14697680601155334, 2007.

Bernacchi, C. J., Singsaas, E. L., Pimentel, C., Portis, A. R., and Long, S. P.: Improved temperature response functions for models of Rubisco-limited photosynthesis, Plant Cell Env, 24, 253-259, https://doi.org/10.1111/j.1365-3040.2001.00668.x, 2001.

Bonan, G.: Climate change and terrestrial ecosystem modeling, Cambridge University Press, Cambridge, UK, xx+438 pp., 2019.

Campbell, G. S., and Norman, J. M.: An introduction to environmental biophysics, Springer, New York City, USA, xv+286 pp., 1998.

Clapp, R. B., and Hornberger, G. M.: Empirical equations for some soil hydraulic properties, Water Resour Res, 14, 601-604, https://doi.org/10.1093/jxb/eri174, 1978.

Dai, Y., Dickinson, R. E., and Wang, Y.-P.: A two-big-leaf model for canopy temperature, photosynthesis, and stomatal conductance, J Climate, 17, 2281-2299, https://doi.org/10.1175/1520-0442(2004)017<2281:Atmfct>2.0.Co;2, 2004.

Dingman, S.: Physical hydrology, Macmillan, New York, USA, 575 pp., 1994.

390 Drake, J. E., Power, S. A., Duursma, R. A., Medlyn, B. E., Aspinwall, M. J., Choat, B., Creek, D., Eamus, D., Maier, C., Pfautsch, S., Smith, R. A., Tjoelker, M. G., and Tissue, D. T.: Stomatal and non-stomatal limitations of photosynthesis for four tree species under drought: A comparison of model formulations, Agr Forest Met, 247, 454-466, https://doi.org/10.1016/j.agrformet.2017.08.026, 2017.

Duursma, R. A., Blackman, C. J., Lopéz, R., Martin-StPaul, N. K., Cochard, H., and Medlyn, B. E.: On the minimum leaf conductance: its role in models of plant water use, and ecological and environmental controls, New Phytol, 221, 693-705, 395 https://doi.org/10.1111/nph.15395, 2019.

Goudriaan, J., and Van Laar, H.: Modelling potential crop growth processes. Current issues in production ecology, Kluwer Academic Publishers, Dordrecht, Netherlands, 978-994 pp., 1994.

Jarvis, P. G., and McNaughton, K. G.: Stomatal control of transpiration: Scaling up from leaf to region, in: Advances in Ecological Research, edited by: MacFadyen, A., and Ford, E. D., Academic Press, Cambridge, USA, 1-49, 1986.

400 Jones, H.: Plants and microclimate: a quantitative approach to environmental plant physiology, Cambridge University Press, Cambridge, UK, 428 pp., 1992.

Katul, G. G., Mahrt, L., Poggi, D., and Sanz, C.: One-and two-equation models for canopy turbulence, Bound-Lay Meteorol, 113, 81-109, https://doi.org/10.1023/B:BOUN.0000037333.48760.e5, 2004.

Katul, G. G., Palmroth, S., and Oren, R.: Leaf stomatal responses to vapour pressure deficit under current and CO_2-enriched 405 atmosphere explained by the economics of gas exchange, Plant Cell Env, 32, 968-979, https://doi.org/10.1111/j.1365-3040.2009.01977.x, 2009.

Kerstiens, G.: Cuticular water permeability and its physiological significance, J Exp Bot, 47, 1813-1832, https://doi.org/10.1093/jxb/47.12.1813, 1996.

Laio, F., Porporato, A., Ridolfi, L., and Rodriguez-Iturbe, I.: Plants in water-controlled ecosystems: active role in hydrologic 410 processes and response to water stress - II. Probabilistic soil moisture dynamics, Adv Water Resour, 24, 707-723, https://doi.org/10.1016/s0309-1708(01)00005-7, 2001.

Leuning, R., Kelliher, F., De Pury, D., and Schulze, E. D.: Leaf nitrogen, photosynthesis, conductance and transpiration: scaling from leaves to canopies, Plant Cell Env, 18, 1183-1200, https://doi.org/10.1111/j.1365-3040.1995.tb00628.x, 1995.

Mäkelä, A., Berninger, F., and Hari, P.: Optimal control of gas exchange during drought: Theoretical analysis, Ann Bot, 77, 415 461-467, https://doi.org/10.1006/anbo.1996.0056, 1996.

Mäkinen, H., Kaseva, J., Trnka, M., Balek, J., Kersebaum, K. C., Nendel, C., Gobin, A., Olesen, J. E., Bindi, M., Ferrise, R., Moriondo, M., Rodríguez, A., Ruiz-Ramos, M., Takáč, J., Bezák, P., Ventrella, D., Ruget, F., Capellades, G., and Kahiluoto, H.: Sensitivity of European wheat to extreme weather, Field Crop Res, 222, 209-217, https://doi.org/10.1016/j.fcr.2017.11.008, 2018.

420 Manzoni, S., Vico, G., Katul, G., Fay, P. A., Polley, W., Palmroth, S., and Porporato, A.: Optimizing stomatal conductance for maximum carbon gain under water stress: a meta-analysis across plant functional types and climates, Funct Ecol, 25, 456-467, https://doi.org/10.1111/j.1365-2435.2010.01822.x, 2011.

Manzoni, S., Vico, G., Porporato, A., and Katul, G.: Biological constraints on water transport in the soil–plant–atmosphere system, Adv Water Resour, 51, 292-304, https://doi.org/10.1016/j.advwatres.2012.03.016, 2013.

425 Medlyn, B., Dreyer, E., Ellsworth, D., Forstreuter, M., Harley, P., Kirschbaum, M., Le Roux, X., Montpied, P., Strassemeyer, J., and Walcroft, A.: Temperature response of parameters of a biochemically based model of photosynthesis. II. A review of experimental data, Plant Cell Env, 25, 1167-1179, https://doi.org/10.1046/j.1365-3040.2002.00891.x, 2002.

Medlyn, B. E., Duursma, R. A., Eamus, D., Ellsworth, D. S., Prentice, I. C., Barton, C. V., Crous, K. Y., De Angelis, P., Freeman, M., and Wingate, L.: Reconciling the optimal and empirical approaches to modelling stomatal conductance, Glob 430 Change Biol, 17, 2134-2144, https://doi.org/10.1111/j.1365-2486.2010.02375.x, 2011.

Milly, P.: Climate, soil water storage, and the average annual water balance, Water Resour Res, 30, 2143-2156, https://doi.org/10.1029/94WR00586, 1994.

Novick, K. A., Ficklin, D. L., Stoy, P. C., Williams, C. A., Bohrer, G., Oishi, A. C., Papuga, S. A., Blanken, P. D., Noormets, A., Sulman, B. N., Scott, R. L., Wang, L., and Phillips, R. P.: The increasing importance of atmospheric demand for ecosystem water and carbon fluxes, Nat Clim Change, 6, 1023, https://doi.org/10.1038/nclimate3114, 2016.

Oren, R., Sperry, J. S., Katul, G. G., Pataki, D. E., Ewers, B. E., Phillips, N., and Schafer, K. V. R.: Survey and synthesis of intra- and interspecific variation in stomatal sensitivity to vapour pressure deficit, Plant Cell Env, 22, 1515-1526, https://doi.org/10.1046/j.1365-3040.1999.00513.x, 1999.

Ridolfi, L., D'Odorico, P., and Laio, F.: Noise-induced phenomena in the environmental sciences, Cambridge University Press, Cambridge, UK, 2011.

Rigby, J. R., and Porporato, A.: Spring frost risk in a changing climate, Geophys Res Lett, 35, https://doi.org/10.1029/2008gl033955, 2008.

Rodriguez-Iturbe, I., Porporato, A., Ridolfi, L., Isham, V., and Cox, D.: Probabilistic modelling of water balance at a point: the role of climate, soil and vegetation, P Roy Soc Lond A Mat, 455, 3789-3805, https://doi.org/10.1098/rspa.1999.0477, 1999.

Saini, H. S., and Aspinall, D.: Abnormal sporogenesis in wheat (*Triticum aestivum* L.) induced by short periods of high temperature, Ann Bot, 49, 835-846, https://doi.org/10.1093/oxfordjournals.aob.a086310, 1982.

Tuzet, A., Perrier, A., and Leuning, R.: A coupled model of stomatal conductance, photosynthesis and transpiration, Plant Cell Env, 26, 1097-1116, https://doi.org/10.1046/j.1365-3040.2003.01035.x, 2003.

Vico, G., and Porporato, A.: Modelling C3 and C4 photosynthesis under water-stressed conditions, Plant Soil, 313, 187-203, https://doi.org/10.1007/s11104-008-9691-4, 2008.

Vico, G., and Porporato, A.: From rainfed agriculture to stress-avoidance irrigation: I. A generalized irrigation scheme with stochastic soil moisture, Adv Water Resour, 34, 263-271, https://doi.org/10.1016/j.advwatres.2010.11.010, 2011.

Vico, G., Manzoni, S., Palmroth, S., Weih, M., and Katul, G.: A perspective on optimal leaf stomatal conductance under CO_2 and light co-limitations, Agr Forest Met, 182, 191-199, https://doi.org/10.1016/j.agrformet.2013.07.005, 2013.

Webber, H., Ewert, F., Kimball, B. A., Siebert, S., White, J. W., Wall, G. W., Ottman, M. J., Trawally, D. N. A., and Gaiser, T.: Simulating canopy temperature for modelling heat stress in cereals, Environ Modell Softw, 77, 143-155, https://doi.org/10.1016/j.envsoft.2015.12.003, 2016.

Wei, Z. W., Yoshimura, K., Wang, L. X., Miralles, D. G., Jasechko, S., and Lee, X. H.: Revisiting the contribution of transpiration to global terrestrial evapotranspiration, Geophys Res Lett, 44, 2792-2801, https://doi.org/10.1002/2016gl072235, 2017.

Wullschleger, S. D.: Biochemical limitations to carbon assimilation in C_3 plants—a retrospective analysis of the A/C_i curves from 109 species, J Exp Bot, 44, 907-920, https://doi.org/10.1093/jxb/44.5.907, 1993.

Zhou, S., Duursma, R. A., Medlyn, B. E., Kelly, J. W., and Prentice, I. C.: How should we model plant responses to drought? An analysis of stomatal and non-stomatal responses to water stress, Agr Forest Met, 182, 204-214, https://doi.org/10.1016/j.agrformet.2013.05.009, 2013.